

# Limits of reactive power compensation of a doubly-fed induction generator-based wind turbine system

Ali Kadhim Abdulabbas<sup>1</sup>, Mazin Abdulelah Alawan<sup>2</sup>, Diyah Kammel Shary<sup>3</sup>

<sup>1</sup>Department of Electrical Engineering, University of Basrah, Basrah, Iraq

<sup>2</sup>Department of Computer Technology Engineering, Shatt Al-Arab University College, Basra, Iraq

<sup>3</sup>Department of Electrical Power Techniques Engineering, Southern Technical University, Basrah, Iraq

## Article Info

### Article history:

Received Oct 8, 2022

Revised Dec 16, 2022

Accepted Feb 14, 2023

### Keywords:

Doubly-fed induction generator

Reactive power limit

Vector control theory

Wind turbine

## ABSTRACT

The doubly-fed induction generator (DFIG) systems feature a significant amount of free power capacity that may be used for reactive power adjustment when they are put into practical use. This change, which is occasionally overlooked, is a significant one. Using DFIG systems for wind turbines (WT), this paper explored strategies for reducing and using reactive power. In order to investigate the power characteristic and how it is regulated in DFIG systems, a mathematical model for the steady-state performance of DFIG WT has been developed and presented. Here is a detailed derivation of the limiting range of DFIG's reactive power capacity as well as the physical constraints on reactive power output. The distribution of the DFIG WT at a distribution network's end is demonstrated by a simulation example. Within this simulation, reactive power management strategy, load fluctuation, and the change in wind speed are all taken into consideration. Due to the possibility of a rise in the voltage at the access point, can concluded that both acceptable and efficient to use DFIG WT's reactive power capabilities as an additional continuous reactive power source for effectiveness.

*This is an open access article under the [CC BY-SA](https://creativecommons.org/licenses/by-sa/4.0/) license.*



## Corresponding Author:

Ali Kadhim Abdulabbas

Department of Electrical Engineering, University Of Basrah

Basrah, Iraq

Email: ali.abdulabbas@uobasrah.edu.iq

## 1. INTRODUCTION

The use of renewable energy sources is quickly becoming a viable option for fulfilling our society's growing need for energy. Interest in producing electricity from renewable resources such hydropower, solar energy, wind energy, geothermal energy, tides, waves, and biomass has significantly increased in recent years [1]–[3]. Everyone agrees that energy plays the biggest role in deciding how wind energy develops. Modern resource depletion techniques employ renewable energy sources to meet the world's growing energy needs since they are more concerned than ever about the state of the environment. Energy production is substantially less expensive today than it was in the past. One example of a potential renewable energy source being researched for the future is wind energy. The usage of doubly-fed induction generator (DFIG) to produce electricity through the utilization of wind energy is common because of the various advantages it offers in contrast to its rivals [4]–[6].

It was discovered that prospective solutions to the problem of grid-connected wind power generation that require the usage of pricey external measures were taken into consideration in various articles [7]–[10] that were investigated. Wind turbines (WTs) connected to the grid operate more efficiently because to reactive power adjustment technologies like static var compensation (SVC) [8] and static synchronous compensator (STATCOM) [9], and they even offer fault riding thanks to their ability to stay connected in the event of

network failures. Other instances include energy storage devices that are used to enhance the quality of wind energy by reducing grid-connected power swings. Along with contributing to the creation of active power, WTs also need to manage reactive and active power. The current WT is able to adjust active and reactive power independently of one another as a result of the modern power electronic converters that come with it [10].

According to Engelhardt *et al.* [11], the constraints of the steady-state reactive power generation capabilities for a typical WT system employing the doubly fed induction generator are thoroughly examined. The parameters of the machine and the control system were determined using data provided by the manufacturer, and the results of the simulation were designed to be as realistic a reflection of the actual world as they could be. DFIG-based WT are increasingly common because of their advantageous cost-performance characteristic, which is essentially the consequence of the need for a much lower converter rating in comparison to the machine rating. This makes DFIG-based WT more appealing to consumers. However, the results of this study do not refer to a change in wind speed and how it affects the capacity of the reactive power.

A reliable adaptive sliding mode controller (ASMC) is suggested in the study [12] to manage the power flow of the WT based on DFIG under varying wind speed. The Lyapunov stability theorem is used to compute the controller's adaptive gains. The switching surfaces of state power faults are defined by two integral functions. To demonstrate the efficacy of the recommended technique under machine parameter uncertainties, a comparison between the sliding mode control (SMC) and the field-oriented control based on proportional integral (PI) controllers is done. The fact that this method involves a lot of tough computations and is challenging to use is one of its drawbacks. This technique also lacks an explanation for what transpires to the rotor voltage when the rotor's reactive power is altered.

The study discussed in reference [13] uses the DFIG at the operational point to examine the steady-state reactive power capabilities of a typical WT system. This study provides a thorough explanation of how power losses and junction temperatures are calculated for converters. Even though the reactive power capacity value has improved, the overall number of electronic components has grown, which results in large power losses and makes management difficult.

Haidi *et al.* [14] offers a synthesis effort based on an updated evaluation of the implemented wind projects and seeks to evaluate the achievement of Morocco's national energy policy, which intends to attain 42% of renewable energy by 2020, with wind energy accounting for 14% of the total energy mix. Additionally, it attempts to demonstrate how wind energy integration affects energy independence, industrial integration, and CO<sub>2</sub> emissions reduction. The purpose of the paper [15] is to provide a quantitative and qualitative analysis of the growth of wind energy in the world, looking at its development over the past ten years, its distribution among major regions and nations, and its contribution to the world's electricity mix while providing an evaluation of the most potent wind farms on the planet. The influence on carbon dioxide emissions reduction, employment development, and electric energy independence are the main points of discussion, as well as the outlook for 2050. The optimal coordination problem employing digital DOCRs with standard characteristics in accordance with IEC60-255 is addressed in the paper [16] through a comparative evaluation of the optimization strategies suggested in the literature. The three most effective and reliable optimization techniques-particle swarm optimization (PSO), genetic algorithm (GA), and differential evolution (DE), are taken into consideration for this aim.

The extracting and exploitation of the reactive power competency of DFIG WT are the topics that are investigated in this paper. In the first step, the power characteristics and relations of power transfer in DFIG systems are provided [17]–[22]. This is accomplished using a mathematical model of a DFIG WT's steady state performance. The second step is to identify the reactive power capacity restriction range of the DFIG, as well as reactive power generation limitations such as stator current, stator voltage, and rotor current. Finally, a simulated example of how to disseminate the DFIG WT at the end of a distribution network is provided. The voltage rate at the access point is raised in this example, demonstrating that using DFIG WT's reactive power capabilities as a new classification reactive power source for utilities is both practical and effective.

## 2. METHOD

### 2.1. Characteristics of the DFIG WT

A WT, a grid-connected, DFIG, and a back-to-back (BTB) converter make up a typical wind power system. In dissimilarity to the stator side of DFIG, which is directly coupled to the grid, the rotor side of DFIG is connected via a BTB converter (rotor-side converter (RSC) and grid-side converter's (GSC)). Figure 1 depicts the power stage of the DFIG WT. The following symbols have the following meanings [7]: the mechanical energy produced by a WT; abbreviated  $P_w$ ,  $P_s$  and  $Q_s$  are the stator's active and reactive powers, respectively. Rotor side reactive and active powers are denoted by the symbols  $P_r$  and  $Q_r$ . The GSC active and reactive powers are denoted by  $P_{gr}$  and  $Q_{gr}$ . The entire quantity of active and reactive electricity that enters the grid is denoted by the symbols  $P_N$  and  $Q_N$ . In order to manage the aerodynamics of the mechanical wind power

( $P_w$ ), WTs use a technique based on the blade pitch angle. When the wind cuts over the blade's surface  $A$  at a speed of  $v_v$ , kinetic energy is released [23]–[26].

$$p_v = \frac{1}{2} \rho A v_v^3 \tag{1}$$

Where  $\rho$  is the air density. Part of this power comes out of the WT using the power coefficient ( $C_p$ ) at the following [27], [28].

$$P_w = \frac{1}{2} \rho \pi R^2 v_v^3 C_p \tag{2}$$

Where  $R$  is the WT's radial distance. The power coefficient ( $C_p$ ) depends on the tip speed ratio  $= \frac{R \Omega_t}{v_v}$ , so  $\Omega_t$  is the rotor's rotational speed. Theoretical maximum value of  $C_p$  is given by the Betz limit [19] then ( $C_{p,theo.max}$ . equal 59.3% at pitch angle ( $\beta$ ) is 4 degree)  $C_p$  is shown in Figure 2.

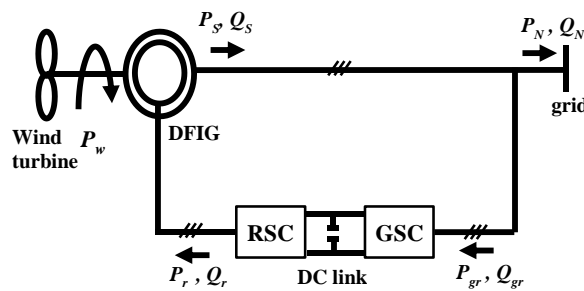


Figure 1. Active and reactive powers in WT system

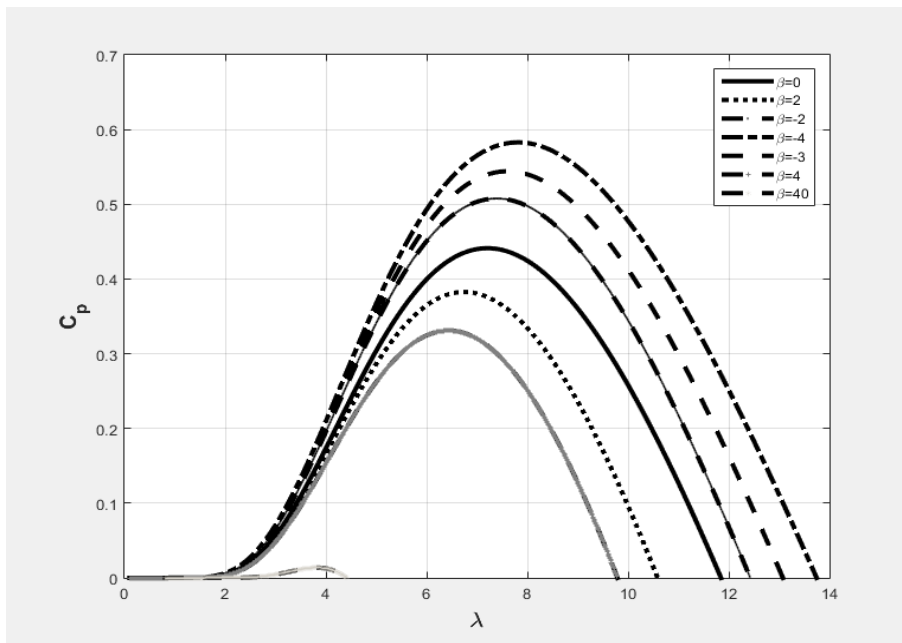


Figure 2. The power coefficient versus tip speed ratio curves

In WT, the relationship between the power generated by the turbine and the wind speed is shown in Figure 3, where the curve is divided into three sections according to the wind speed, the first section at a speed less than the cutting speed  $\omega_{cut}$ , and in which no power is generated from the turbine, while in the second section it is located between  $v_{min}$  and  $v_{max}$  where the maximum power point tracking (MPPT) technology is

used. When the output speed  $\omega_{out}$  is reached, the power is to the maximum obtained from the WT for that third section after the output speed reach the maximum wind speed  $v_{max}$ . In addition to the stator windings ( $P_s$ ), the rotor windings are also used to transmit power from the DFIG WT system to the grid ( $P_r$ ). The bulk of the energy is delivered to the grid via the stator windings, while the remaining portion is communicated through BTB converters via the rotor windings.

Because the rotor's active power is generally proportional to both the slip and the stator's active power, the rotor's active power is equal to the quantity of  $s P_s$  and flows in both directions through the BTB converters. This permits the active power to span the widest feasible range of work, from sub-to super-synchronous. Using the concept of energy conservation and disregarding power losses through power converters, the rotor power  $P_r$  equals the power of the grid side converter  $P_{gr}$  [29]–[32]. The connection between active powers in the system may be described as given in (3), using the power direction illustrated in Figure 1 and ignoring power losses in the DFIG system.

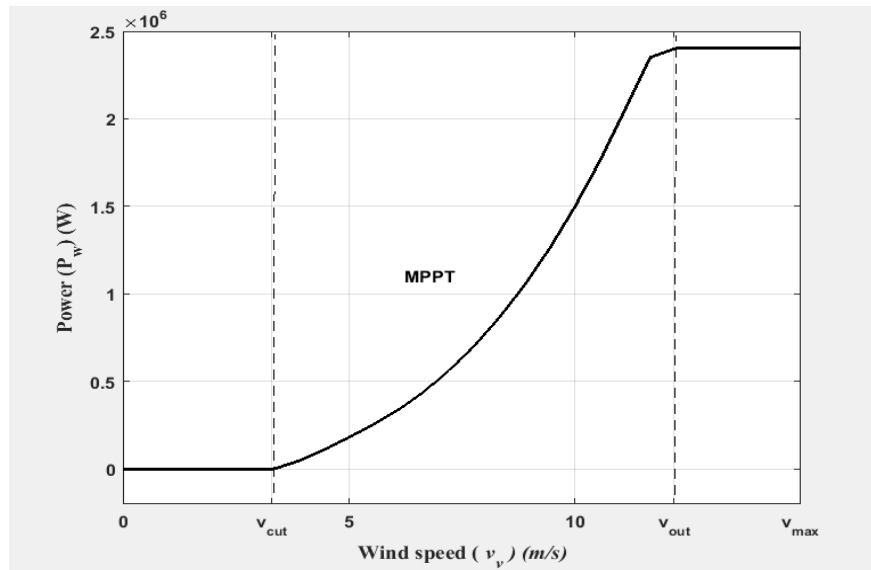


Figure 3. Wind power against the wind speed curve

$$P_N = P_S - P_{gr} = P_S - P_r = P_w \quad (3)$$

$$P_r \cong -s P_S \quad (4)$$

$$P_w \cong (1 - s)P_S = \frac{s}{1-s} P_r \quad (5)$$

The reactive powers  $Q_r$  and  $Q_{gr}$  are independent of one another since RSC and GSC are connected via a DC connection. The following is done to create reactive power for the grid:

$$Q_N = Q_S - Q_{gr} \quad (6)$$

A stator-flux orientation control reference frame may be used to modify the active and reactive powers separately [5]. The q-axis rotor current controls the active power  $P_S$  so that the turbine can harness the most power possible from the wind. The management of the d-axis rotor current is fundamentally distinct from the regulation of the reactive power  $Q_S$ , on the other hand. This role should be carried out and controlled by the RSC. The grid ac voltage-oriented reference frame is used at GSC to manage and maintain the DC-link voltage. Additionally, the current in the q-axis, which may also be used to regulate the reactive power generated by the GSC, regulates the DC-link regulation ( $Q_{gr}$ ).

## 2.2. Equivalent circuit and reactive power limit of DFIG-WT

Figure 4 depicts the DFIG equivalent circuit for each phase. The phasor diagram for the mathematical model needed to determine the DFIG WT's reactive power limit must be drawn from this circuit. The mathematical model is represented by the two-voltage equation on both sides in the steady-state of the stator part and the rotor part as given in (7) and (8).

$$\vec{v}_s = \vec{I}_s(r_s + jx_s) + (\vec{I}_s + \vec{I}_r)jx_m \tag{7}$$

$$\vec{v}_r = \vec{I}_r\left(\frac{r_r}{s} + jx_r\right) + (\vec{I}_s + \vec{I}_r)jx_m \tag{8}$$

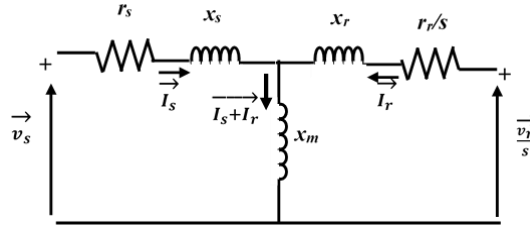


Figure 4. DFIG's equivalent circuit in phasor form

When (7) applied, the stator resistance may be ignored and the stator DFIG current can be represented as (9):

$$\vec{I}_s = \frac{-j\vec{v}_s - x_m \vec{I}_r}{x_s + x_m} \tag{9}$$

The power that is supplied to the stator ( $S_s$ ), which is measured via the stator voltage, is the reference vector.

$$S_s = -P_s - jQ_s = \frac{3jV_s^2 - 3jV_s x_m I_{dr} - 3V_s x_m I_{qr}}{x_s + x_m} \tag{10}$$

Then using  $L_s \leq L_m$

$$I_{dr} = \frac{2 Q_s L_s}{3 V_s L_m} + \frac{V_s}{L_m \omega_s} \tag{11}$$

and

$$I_{qr} = \frac{2 L_s P_s}{3 V_s L_m} \tag{12}$$

The stator field orientation theory is expressed in (11) and (12) in a rotating frame with a synchronous d-q axis. The following factors limit the maximum rotor current  $i_{rmax}$  (13).

$$\left(\frac{2 Q_s L_s}{3 V_s L_m} + \frac{V_s}{L_m \omega_s}\right)^2 + \left(\frac{2 L_s P_s}{3 V_s L_m}\right)^2 \leq i_{rmax}^2 \tag{13}$$

The  $P_s$  is particular, and then fined the range of  $Q_s$  at any operation point of the DFIG so (13) can be represented by:

$$Q_s = -\frac{3 V_s^2}{2 \omega_s L_s} \mp \sqrt{\left(\frac{3 V_s L_m}{2 L_s} i_{rmax}\right)^2 - P_s^2} \tag{14}$$

So, (14) can be expressed by maximum and minimum stator reactive powers.

$$Q_{smax1} = -\frac{3 V_s^2}{2 \omega_s L_s} + \sqrt{\left(\frac{3 V_s L_m}{2 L_s} i_{rmax}\right)^2 - \left(\frac{P_w}{1-s}\right)^2} \tag{15}$$

$$Q_{smin1} = -\frac{3 V_s^2}{2 \omega_s L_s} - \sqrt{\left(\frac{3 V_s L_m}{2 L_s} i_{rmax}\right)^2 - \left(\frac{P_w}{1-s}\right)^2} \tag{16}$$

By using the maximum stator current  $i_{smax}$  as a limitation, another range of  $Q_s$  is possible.

$$Q_s = \mp \sqrt{S_s^2 - P_s^2}$$

So

$$Q_{smax2} = +\sqrt{(3 V_s i_{smax})^2 - \left(\frac{P_w}{1-S}\right)^2} \quad (17)$$

$$Q_{smin2} = -\sqrt{(3 V_s i_{smax})^2 - \left(\frac{P_w}{1-S}\right)^2} \quad (18)$$

The particular real range of DFIG may be represented by the following:

$$Q_{smax} = \text{minimum} (Q_{smax1}, Q_{smax2}) \quad (19)$$

$$Q_{smin} = \text{minimum} (Q_{smin1}, Q_{smin2})$$

Only a little amount of real power is transmitted through the BTB converter, supposing the maximum apparent power of GSC is  $S_{grmax}$  when the DFIG WT is operating. Therefore, the boundary limit of  $Q_{gr}$  is determined by the restriction  $P_{gr}^2 + Q_{gr}^2 \leq S_{grmax}^2$  indicated in (20).

$$Q_{grmax} = \sqrt{(S_{grmax})^2 - \left(\frac{SP_w}{1-S}\right)^2} \quad (20)$$

$$Q_{grmin} = -\sqrt{(S_{grmax})^2 - \left(\frac{SP_w}{1-S}\right)^2}$$

Therefore, the total reactive power of the network limit by the DFIG WT  $Q_N$  can be given as:

$$Q_{Nmax} = Q_{smax} - Q_{grmin} \quad (21)$$

$$Q_{Nmin} = Q_{smin} - Q_{grmax}$$

Some of the parameters of the limiters in (11) to (21) include the stator current, stator voltage, and rotor current. The DFIG WT system's network limits the stator voltage, the generator design is used to compute the stator current, and the generator and rotor converter designs both have an effect on the rotor current. If the parameters are assumed to be constant and dependent on the generator speed, it is possible to determine the range of reactive power that the stator and rotor portions of the design in Figures 5 and 6 contribute to the network. As shown in Figure 5, the stator current value determines the lower limit while the rotor current value determines the higher limit. As a result, the highest transistor current that the converter is capable of producing limits the magnitude of the rotor current. When the wind speed is lower than usual, the DFIG has the capacity to process reactive power in two directions.

### 2.3. Vector control of DFIG WT

The equations of DFIG are represented by the space vector model in d-q synchronous reference frame as (22):

$$\vec{v}_s^e = r_s \vec{i}_s^e + \frac{d\vec{\psi}_s^e}{dt} + j \omega_s \vec{\psi}_s^e \quad (22)$$

$$\vec{v}_r^e = r_r \vec{i}_r^e + \frac{d\vec{\psi}_r^e}{dt} + j \omega_{sr} \vec{\psi}_r^e$$

Where the slip speed  $\omega_{sr} = \omega_s - \omega_r$

As a result, the fluxes in the stator and rotor may be represented as having the following relationship:

$$\vec{\psi}_S^e = L_S \vec{i}_S^e + L_m \vec{i}_r^e$$

$$\vec{\psi}_r^e = L_m \vec{i}_S^e + L_r \vec{i}_r^e$$
(23)

On both (GSC and RSC) converters, the vector control technique can be used.

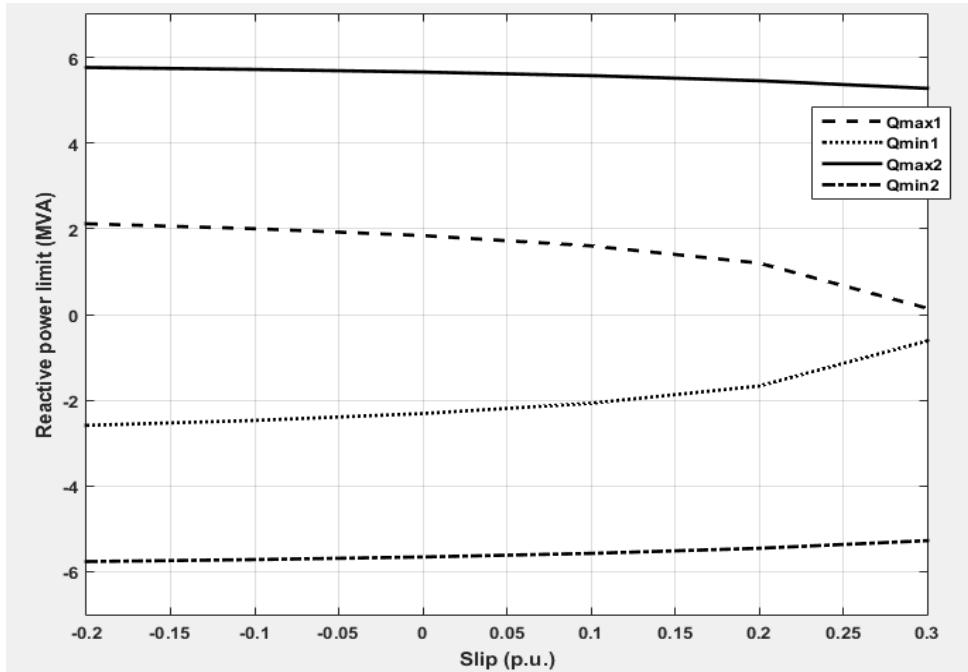


Figure 5. Limit of reactive power of a stator with slip

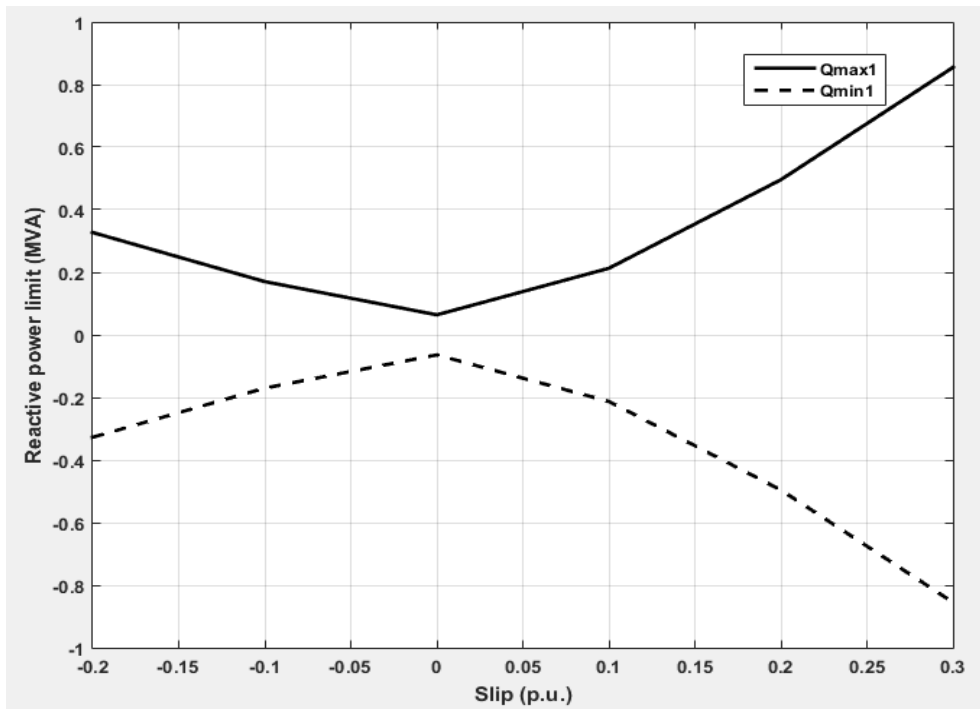


Figure 6. Reactive power limit of DFIG WT

### 2.3.1. Rotor side control

The flux-oriented synchronous reference frame, with the d-axis aligned with the stator flux space vector, can be used to control the vector on the rotor side of the DFIG. In this alignment, the torque or active power PS is proportional to the quadrature rotor current, whereas the direct rotor current is proportional to the stator inactive power QS. Using  $\psi_{qs}=0$  and  $\psi_{ds}=\frac{L_m}{L_s}|\vec{\psi}_s|$ , decompose the rotor voltage represented in (22) and (23) into its constituent parts.

$$\begin{aligned} V_{dr} &= r_r i_{dr} + \sigma L_r \frac{di_{dr}}{dt} - \omega_{sr} \sigma L_r i_{qr} + \frac{L_m}{L_s} \frac{d|\vec{\psi}_s|}{dt} \\ V_{qr} &= r_r i_{qr} + \sigma L_r \frac{di_{qr}}{dt} + \omega_{sr} \sigma L_r i_{dr} + \omega_{sr} \frac{L_m}{L_s} |\vec{\psi}_s| \end{aligned} \quad (24)$$

Where  $\sigma = 1 - \frac{L_m^2}{L_r L_s}$

The derivative of the flux is equal to zero since the stator is directly linked to the grid at a constant AC voltage ( $\frac{d|\vec{\psi}_s|}{dt} = 0$ ). Therefore, according to the final two equations, it is possible to control the current in the rotor component using a synchronous reference frame. Additionally, as shown in Figure 7, the cross terms in (24) aid the control process in regulating the current in the rotor. A simple phase locked loop (PLL) can be used to perform synchronized with the network voltage, thus giving stability to the control process and rejecting distortion of harmonics. Therefore, for the purpose of obtaining an angle  $\theta_s$  that is subtracted from  $90^\circ$  to the estimated angle as shown in Figure 8. In order to complete the DQ transformation, it is necessary to subtract  $\theta_m$  from  $\theta_s$  in order to get the angle  $\theta_r$ . The torque expression can be made simpler by employing the stator flux orientation frame in the fashion shown in:

$$T_{em} = -\frac{3}{2} p \frac{L_m}{L_s} |\vec{\psi}_s| i_{qr} \quad (25)$$

Where  $p$  is the number of poles on the generator. Hence, the torque may influence the current  $i_{qr}$ , and as a consequence, the direct current  $i_{dr}$  could regulate both the machine's active and reactive power using the following (26):

$$Q_s = -\frac{3}{2} \omega_s \frac{L_m}{L_s} |\vec{\psi}_s| \left( i_{dr} - \frac{|\vec{\psi}_s|}{L_m} \right) \quad (26)$$

### 2.3.2. Grid side control

Here, the control of the GSC is covered. A grid-side dynamic model based on space vector theory is created first, and then the control of the GSC is examined. Investigated is the vector control technique. The grid voltage space vector is aligned with a rotational reference frame (DQ) that is used. By controlling the reactive power exchange and the DC bus voltage, the GSC is able to achieve its two main goals of ensuring power supply through the converter and regulating the DC bus voltage. The following equations describe the grid-side dynamic model in the dq-reference frame by using the vector control technique the grid voltage yield  $v_{dG} = |\vec{v}_G^e|$  and  $v_{qG} = 0$ .

$$\begin{aligned} v_{df} &= r_f i_{dG} + L_f \frac{di_{dG}}{dt} + |\vec{v}_G^e| - \omega_s L_f i_{qG} \\ v_{qf} &= r_f i_{qG} + L_f \frac{di_{qG}}{dt} + \omega_s L_f i_{dG} \end{aligned} \quad (27)$$

Where  $v_{df}$  and  $v_{qf}$  are the voltages that the grid side converter imposes and  $v_{dG}$  and  $v_{qG}$  are the grid voltage with constant amplitude and frequency. Active and reactive power calculations are simplified by this alignment of the grid's voltage. Thus, (28) used to conclude the total of active and reactive power flows into or out of the grid.

$$P_G = \frac{3}{2} |\vec{v}_G^e| i_{dG} \quad (28)$$



$$Q_G = -\frac{3}{2} |\vec{v}_G^e| i_{qG}$$

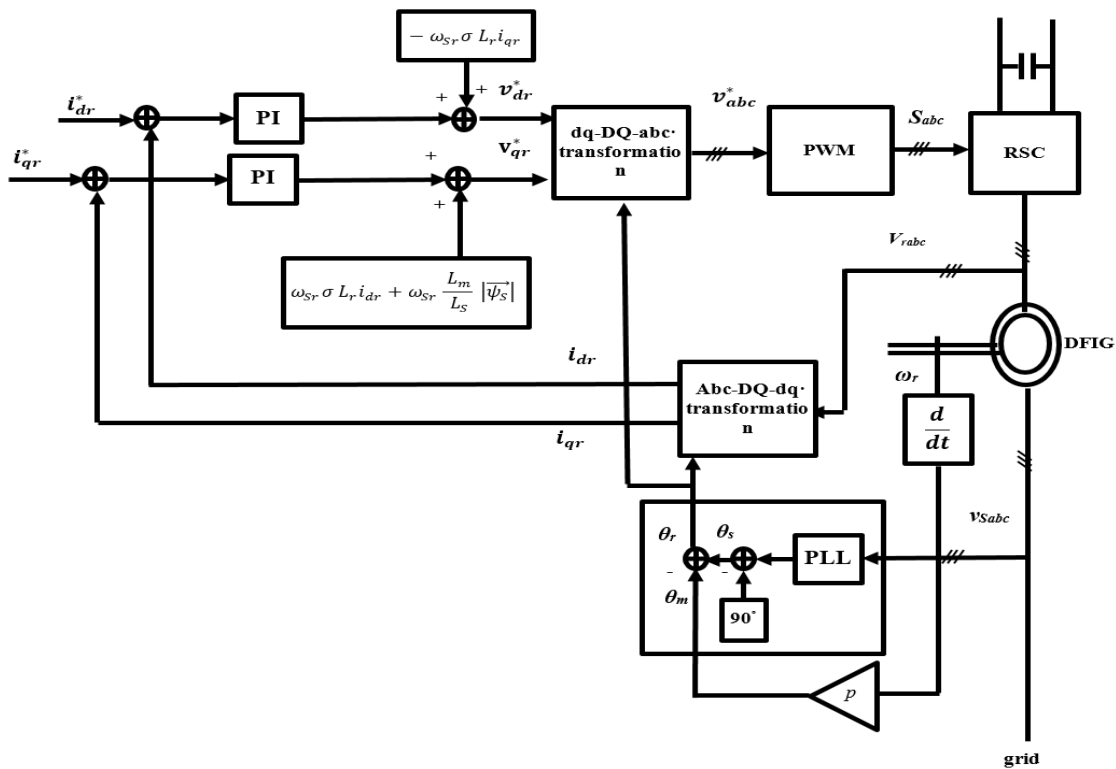


Figure 7. Rotor-side vector control

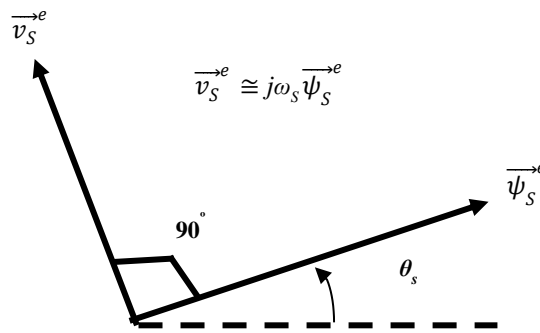


Figure 8. Orientation of stator voltage

It is vital to remember that under ideal conditions, the voltage terms of these latter two equations stay unaltered; this implies that a decoupled link between the current dq components and the active and reactive powers has been accomplished. The active and reactive power estimated in the converter terminals, on the other hand, is not the same as the power computed in the grid terminals. The power produced by the converter should be defined using the following (29):

$$P_f = \frac{3}{2} (r_f (|\vec{i}_G^e|)^2 + |\vec{v}_G^e| i_{dG})$$

$$Q_f = \frac{3}{2} (\omega_s L_f (|\vec{i}_G^e|)^2 - |\vec{v}_G^e| i_{qG})$$
(29)

A schematic of the control block diagram and a basic block diagram of the grid-side system are shown in Figure 9. In this diagram, the DC connection, which is mostly provided by a capacitor, calls for DC-bus management. As a result, before being supplied into the grid, the active power flow of the rotor must first pass across the DC connection. This active power flow through the converters is made feasible by setting the  $V_{bus}$  variable to a constant value, which also ensures that the DC voltage requirements for the grid-side and rotor-side converters are met. Another element that may be managed with the help of this system is the reactive power exchange with the grid (QG).

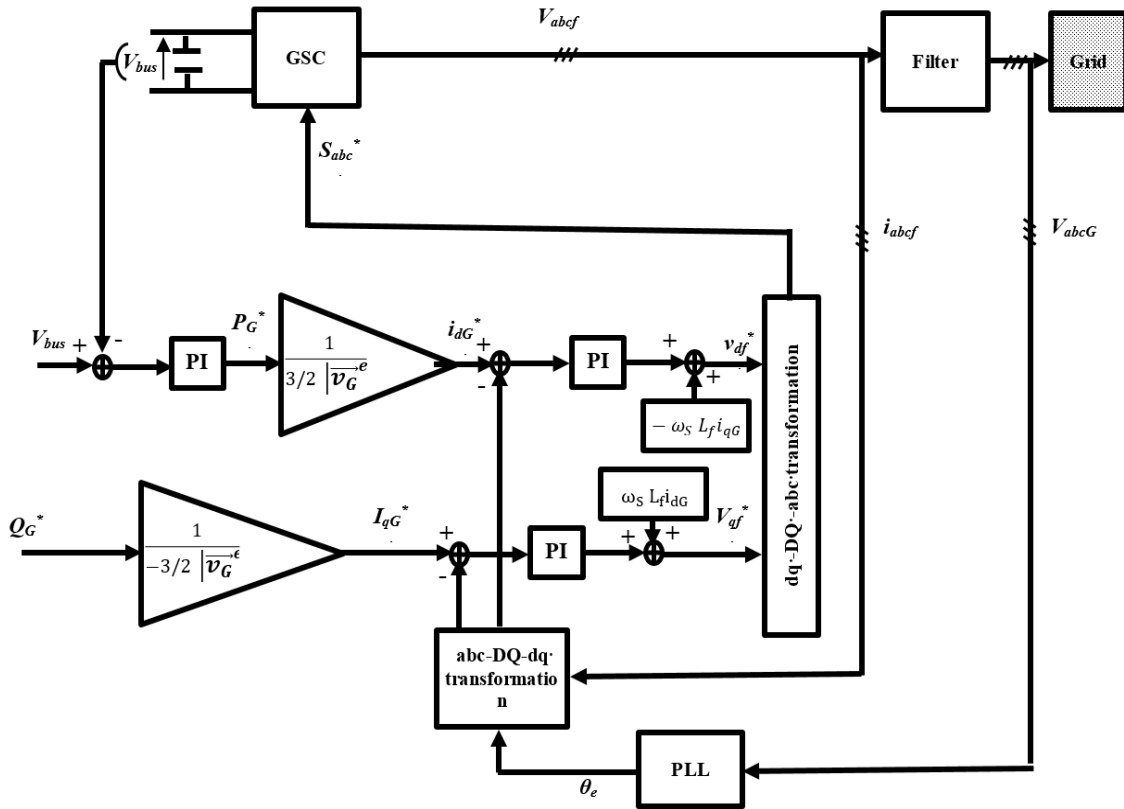


Figure 9. Grid-side vector control

### 3. RESULTS AND DISCUSSION

The mathematical formulae allow for the drawing of curves of the optimum rotor fault current and the needed rotor voltage output rather than the control parameters. By running the previous system on the basis of calculating the capacity of the rotor with a MATLAB/Simulink program, the many components in DFIG were depicted in Table 1. This was done so that the capacity of the rotor could be determined by given at  $C_p$  equal 0.44. Using a sudden increase in wind speed from 5 m/s to 11 m/s at a time interval of 6 sec, and thus the work moving to the MPPT curve in Figure 3, and then using a subsequent increase in wind speed from 11 to 13 m/s, and thus the work moving to the maximum power generated by the WT. Figure 10 shows the increase of generator speed and the reference value of speed, while Figures 11-13 depict the evolution of torque, rotor current, and rotor side voltage, respectively. In these figures, we can see that the value of the rotor part's current is maintained within the permitted range. Similarly, the rotor part's voltage is also maintained within the allowed range. This is done to protect the semiconductor element of the RSC circuit from values that are too high. In addition, the reactive power is managed in a way that ensures that both the capacity of the DFIG and the capacity of the RSC are taken into consideration.

The simulation experiment displays both the grid and the rotor side's steady state and transient performance while they are under the control of the vector control was discussed in the previous section. In order to retain the BTB converters' capacity to operate in equilibrium, Figure 14 represents the DC bus connection voltage and illustrates its stability value. These converters are linked to the power exchange with the grid. Quantities on the network side, such as the change in reactive power on the rotor side and the power provided to the grid from the GSC switch within the work limitations, are depicted in Figure 15(a) and (b).

This is due to the rotor's ability to provide the DFIG's nominal power throughout the simulation. This is due to the rotor's ability to provide the DFIG's nominal power throughout the simulation. It is capable of controlling the voltage at the network and prevent voltage surges when a fault develops at one or more points in the network by calculating the value of the reactive power supplied by the generator.

Table 1. The parameters of DFIG

| Variable   | Value | Unit    | Description                 |
|------------|-------|---------|-----------------------------|
| $r_s$      | 2.6   | mΩ      | Stator resistance           |
| $r_r$      | 2.9   | mΩ      | Rotor resistance            |
| $L_s, L_r$ | 2.587 | mH      | Stator and rotor inductance |
| $L_m$      | 2.5   | mH      | Magnetization inductance    |
| $L_f$      | 400   | μH      | Filter inductance           |
| $p$        | 4     |         | Pole of the generator       |
| $\omega_s$ | 377   | Rad/sec | Synchronous frequency       |

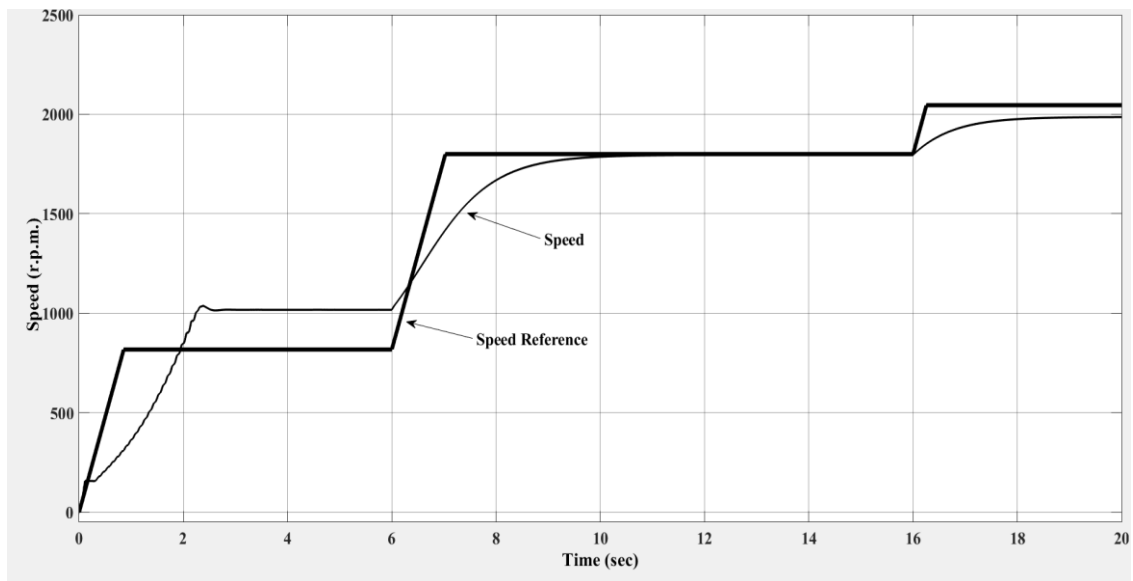


Figure 10. Simulation of generator speed

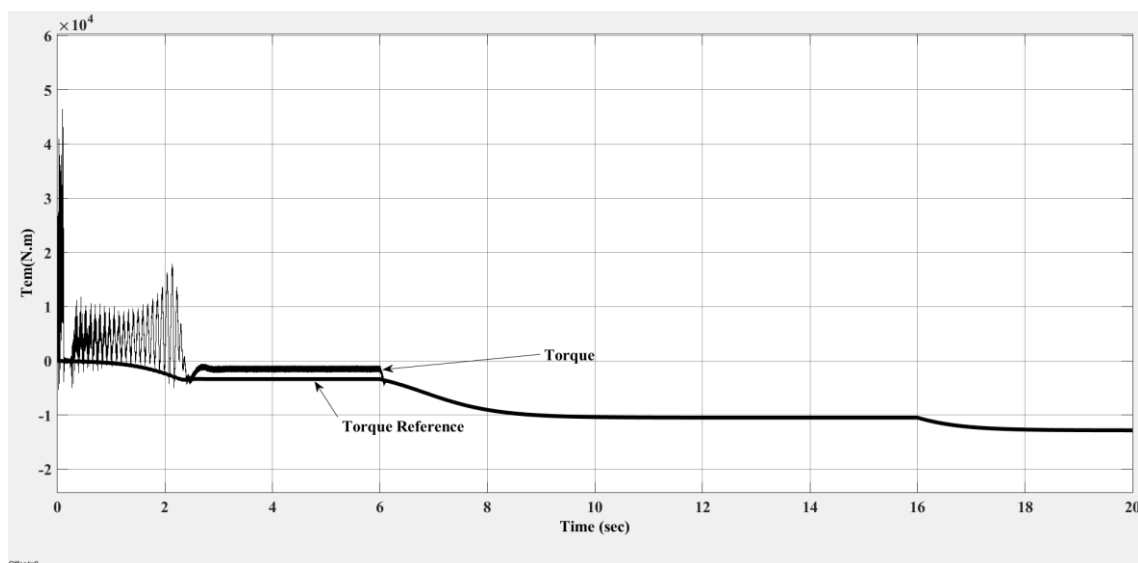


Figure 11. Simulation of generator torque

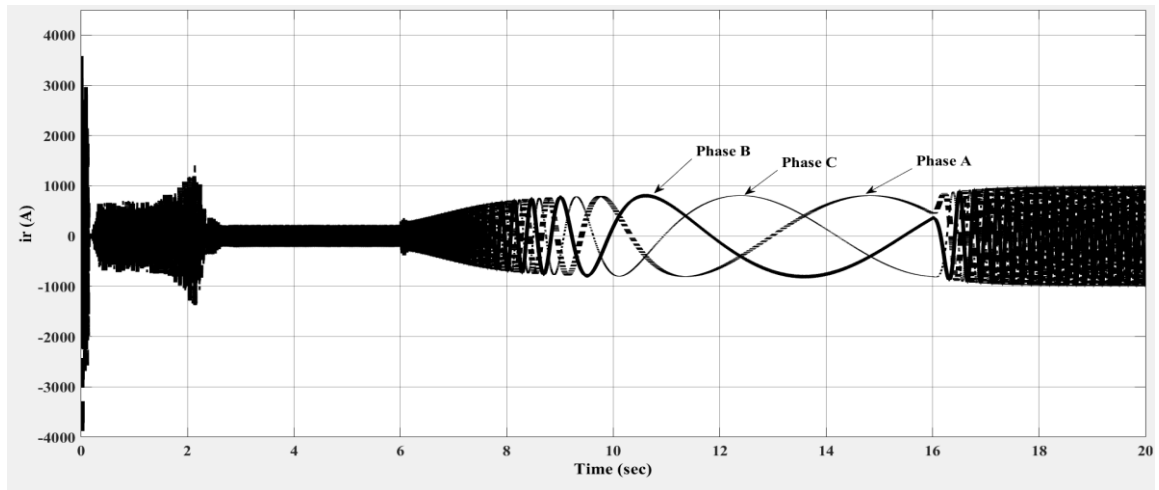


Figure 12. Simulation of rotor current

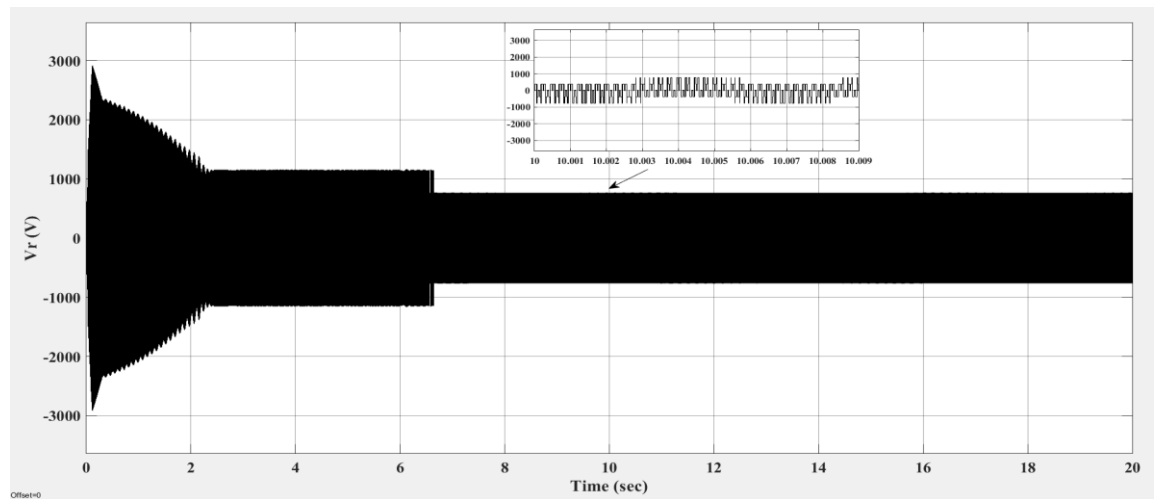


Figure 13. Rotor voltage of DFIG

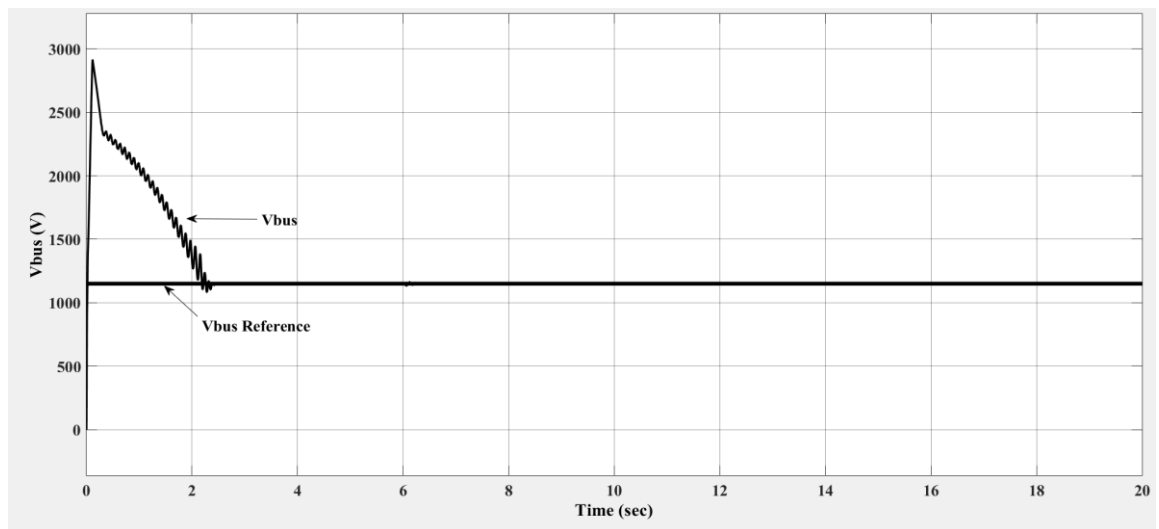
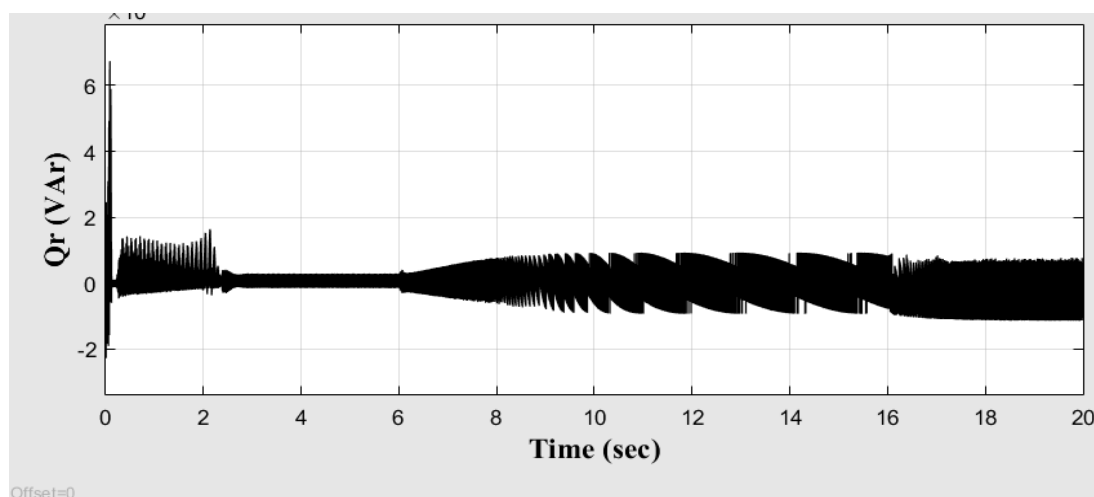
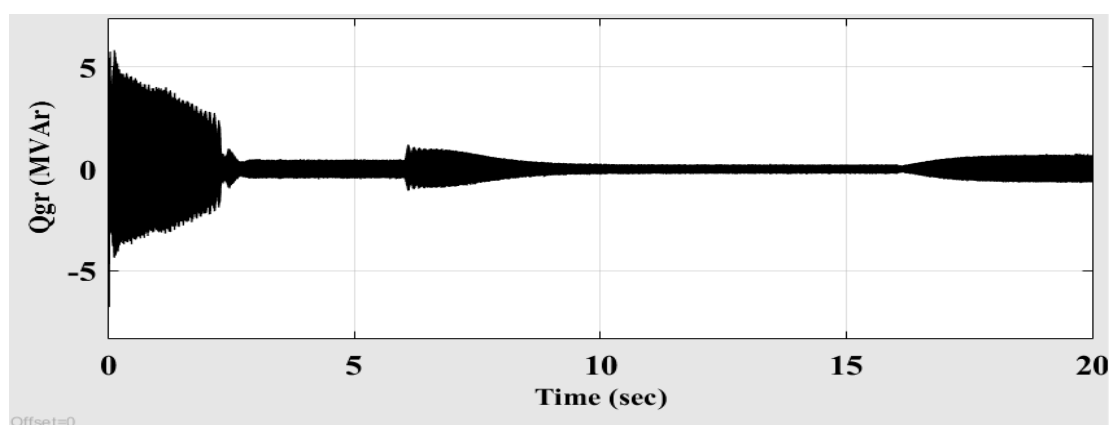


Figure 14. Simulation of DC bus link vottage



(a)



(b)

Figure 15. The change in reactive power (a) Rotor side and (b) Grid side.

#### 4. CONCLUSION

DFIG-WT has a significant potential reactive power capacity as well as flexible control features, which enable it to control the decoupling of both reactive and active power, as may be inferred from the operating principle and the power relationship within it. When calculating the reactive power produced by DFIG-WTs and the limiting factor for the reactive power limit, the three primary variables are stator current, rotor current, and stator voltage. In addition to being defined by their precise range while the turbine is running, the currents of the stator and rotor are also determined by design. The connecting grid regulates the stator voltage. This paper described example of decreasing and exploiting DFIG-WT reactive power capacity, regulating the reactive power for the purpose of controlling voltage improves the load voltage level and reduces line loss. The range of reactive power of WT between 0.07 MVA to -0.06 MVA at slip -0.05 to 0.05. The primary takeaway from the study is that it is advantageous and practical to make use of the DFIG WT's potential reactive power capabilities. The major objective of this research, as well as advantageous and practicable to use the DFIG WT's future reactive power capabilities.

#### ACKNOWLEDGEMENTS




Special thanks to Shatt Al-Arab University College for its scientific and substantial support, and also, we would like to thank the journal staff for their valuable notes to make this paper in well form.

#### REFERENCES




- [1] J. M. Morales, L. Baringo, A. J. Conejo, and R. Mi'nguez, "Probabilistic power flow with correlated wind sources," *IET Generation, Transmission and Distribution*, vol. 4, no. 5, p. 641, 2010, doi: 10.1049/iet-gtd.2009.0639.
- [2] T. Haidi and B. Cheddadi, "Wind energy integration in Africa: development, impacts and barriers," *International Journal of Electrical and Computer Engineering (IJECE)*, vol. 12, no. 5, p. 4614, Oct. 2022, doi: 10.11591/ijece.v12i5.pp4614-4622.

- [3] S. Paaso, "Mixed integer linear programming based algorithms for wind farm layout optimization," Master's Programme in Advanced Energy Solutions, Aalto University, Finlandia, 2022.
- [4] M. Debouza and A. Al-Durra, "Grid Ancillary Services From Doubly Fed Induction Generator-Based Wind Energy Conversion System: A Review," *IEEE Access*, vol. 7, pp. 7067–7081, 2019, doi: 10.1109/access.2018.2890168.
- [5] A. C. Cepeda and M. A. Rios, "Bulk power system availability assessment with multiple wind power plants," *International Journal of Electrical and Computer Engineering (IJECE)*, vol. 11, no. 1, p. 27, Feb. 2021, doi: 10.11591/ijece.v11i1.pp27-36.
- [6] S. B. Utomo, I. Setiawan, B. Fajar, S. H. Winoto, and A. Marwanto, "Optimizing of the installed capacity of hybrid renewable energy with a modified MPPT model," *International Journal of Electrical and Computer Engineering (IJECE)*, vol. 12, no. 1, p. 73, Feb. 2022, doi: 10.11591/ijece.v12i1.pp73-81.
- [7] D. Zhi, L. Xu, and B. W. Williams, "Model-Based Predictive Direct Power Control of Doubly Fed Induction Generators," *IEEE Transactions on Power Electronics*, vol. 25, no. 2, pp. 341–351, Feb. 2010, doi: 10.1109/tpel.2009.2028139.
- [8] S. Chakraborty, S. Mukhopadhyay, and S. Biswas, "Coordination of D-STATCOM and SVC for Dynamic VAR Compensation and Voltage Stabilization of an AC Grid Interconnected to a DC Microgrid," *IEEE Transactions on Industry Applications*, vol. 58, no. 1, pp. 634–644, Jan. 2022, doi: 10.1109/tia.2021.3123264.
- [9] R. K. Varma and R. Salehi, "SSR Mitigation With a New Control of PV Solar Farm as STATCOM (PV-STATCOM)," *IEEE Transactions on Sustainable Energy*, vol. 8, no. 4, pp. 1473–1483, Oct. 2017, doi: 10.1109/tste.2017.2691279.
- [10] J. S. Sathyanarayanan and A. S. Kumar, "Doubly Fed Induction Generator Wind Turbines with Fuzzy Controller: A Survey," *The Scientific World Journal*, vol. 2014, p. e252645, Jun. 2014, doi: 10.1155/2014/252645.
- [11] S. Engelhardt, I. Erlich, J. Kretschmann, and F. Shewarega, "Reactive Power Capability of Wind Turbines Based on Doubly Fed Induction Generators," *IEEE Transactions on Energy Conversion*, vol. 26, no. 1, pp. 364–372, Mar. 2011, doi: 10.1109/tec.2010.2081365.
- [12] O. Zamzoum, Y. El, M. Errouha, A. Derouich, and A. El, "Active and Reactive Power Control of Wind Turbine based on Doubly Fed Induction Generator using Adaptive Sliding Mode Approach," *International Journal of Advanced Computer Science and Applications*, vol. 10, no. 2, 2019, doi: 10.14569/ijcsa.2019.0100252.
- [13] M. Z. Sujod and I. Erlich, "Reactive power capability of DFIG based wind turbine around synchronous operating point with two-level and three-level NPC converter," in *2013 IEEE Grenoble Conference*, Jun. 2013, doi: 10.1109/ptc.2013.6652099.
- [14] T. Haidi, B. Cheddadi, F. E. Mariami, Z. E. Idrissi, and A. Tarrak, "Wind energy development in Morocco: Evolution and impacts," *International Journal of Electrical and Computer Engineering (IJECE)*, vol. 11, no. 4, p. 2811, Aug. 2021, doi: 10.11591/ijece.v11i4.pp2811-2819.
- [15] T. Haidi and B. Cheddadi, "State of wind energy in the world: evolution, impacts and perspectives," *International Journal on Technical and Physical Problems of Engineering (IJTPE)*, vol. 14, no. 51, pp. 347–352, Jun. 2022.
- [16] Z. E. Idrissi, T. Haidi, F. Elmariami, and A. Belfqih, "Comparative study of optimization methods for optimal coordination of directional overcurrent relays with distributed generators," *IAES International Journal of Artificial Intelligence (IJ-AI)*, vol. 12, no. 1, p. 209, Mar. 2023, doi: 10.11591/ijai.v12.i1.pp209-219.
- [17] S. M. M. Aval, A. Ahadi, and H. Hayati, "A novel method for reliability and risk evaluation of wind energy conversion systems considering wind speed correlation," *Frontiers in Energy*, vol. 10, no. 1, pp. 46–56, Nov. 2015, doi: 10.1007/s11708-015-0384-4.
- [18] M. Tazil, V. Kumar, R. C. Bansal, S. Kong, Z. Y. Dong, and W. Freitas, "Three-phase doubly fed induction generators: an overview," *IET Electric Power Applications*, vol. 4, no. 2, p. 75, 2010, doi: 10.1049/iet-epa.2009.0071.
- [19] S. Sahoo, B. Subudhi, and G. Panda, "Comparison of Output Power Control Performance of Wind Turbine using PI, Fuzzy Logic and Model Predictive Controllers," *International Journal of Renewable Energy Research (IJRER)*, vol. 8, no. 2, Jun. 2018.
- [20] J. Tian, C. Su, and Z. Chen, "Reactive power capability of the wind turbine with Doubly Fed Induction Generator," in *IECON 2013 - 39th Annual Conference of the IEEE Industrial Electronics Society*, Nov. 2013, doi: 10.1109/iecon.2013.6699999.
- [21] L. Riachy, H. Alawieh, Y. Azzouz, and B. Dakyo, "A Novel Contribution to Control a Wind Turbine System for Power Quality Improvement in Electrical Networks," *IEEE Access*, vol. 6, pp. 50659–50673, 2018, doi: 10.1109/access.2018.2869479.
- [22] J. Lee, G. Jang, E. Muljadi, F. Blaabjerg, Z. Chen, and Y. C. Kang, "Stable Short-Term Frequency Support Using Adaptive Gains for a DFIG-Based Wind Power Plant," *IEEE Transactions on Energy Conversion*, vol. 31, no. 3, pp. 1068–1079, Sep. 2016, doi: 10.1109/tec.2016.2532366.
- [23] H. Wang, Z. Chen, and Q. Jiang, "Optimal control method for wind farm to support temporary primary frequency control with minimised wind energy cost," *IET Renewable Power Generation*, vol. 9, no. 4, pp. 350–359, May 2015, doi: 10.1049/iet-rpg.2014.0045.
- [24] H. Attar, M. A. Kamarposhti, and A. A. A. Solyman, "Impacts of integration of wind farms on voltage stability margin," *International Journal of Electrical and Computer Engineering (IJECE)*, vol. 12, no. 5, p. 4623, Oct. 2022, doi: 10.11591/ijece.v12i5.pp4623-4631.
- [25] M. Fannakh, M. L. Elhafyani, S. Zouggar, and H. Zahboune, "Overall fuzzy logic control strategy of direct driven PMSG wind turbine connected to grid," *International Journal of Electrical and Computer Engineering (IJECE)*, vol. 11, no. 6, p. 5515, Dec. 2021, doi: 10.11591/ijece.v11i6.pp5515-5529.
- [26] A. Gourma, A. Berdai, and M. Reddak, "The transient stability analysis of wind turbines interconnected to grid under fault," *International Journal of Electrical and Computer Engineering (IJECE)*, vol. 10, no. 1, p. 600, Feb. 2020, doi: 10.11591/ijece.v10i1.pp600-608.
- [27] P. Beiter, M. Elchinger, and T. Tian, "2016 Renewable Energy Data Book," National Renewable Energy Lab. (NREL), Golden, CO (United States), United States, DOE/GO-102016-4904, Dec. 2017, doi: 10.2172/1466900.
- [28] N. Nguyen and J. Mitra, "Reliability of Power System with High Wind Penetration Under Frequency Stability Constraint," *IEEE Transactions on Power Systems*, vol. 33, no. 1, pp. 985–994, Jan. 2018, doi: 10.1109/tpwrs.2017.2707475.
- [29] B. Shakerighadi, E. Ebrahimzadeh, F. Blaabjerg, and C. L. Bak, "Large-Signal Stability Modeling for the Grid-Connected VSC Based on the Lyapunov Method," *Energies*, vol. 11, no. 10, p. 2533, Sep. 2018, doi: 10.3390/en1102533.
- [30] A. Nair, K. Murali, S. P. Anbuudayasankar, and C. V. Arjunan, "Modelling and Optimising the Value of a Hybrid Solar-Wind System," *IOP Conference Series: Materials Science and Engineering*, vol. 197, p. 012035, May 2017, doi: 10.1088/1757-899x/197/1/012035.
- [31] K. Shah, V. Gaur, S. Joshi, and N. Patel, "Maximum Power Point Tracking Methods for Wind and Solar Conversion Systems for Standalone Generation PSIM based Perturb and Observe Method," in *International Journal of Engineering Research and Development (IJERD)*, Apr. 2015, pp. 46–54.
- [32] O. O. Mengi and I. H. Altas, "A New Energy Management Technique for PV/Wind/Grid Renewable Energy System," *International Journal of Photoenergy*, vol. 2015, pp. 1–19, 2015, doi: 10.1155/2015/356930.




**BIOGRAPHIES OF AUTHORS**

**Ali Kadhim Abdulabbas**    was born in Basrah, Iraq in 1975. He received his B.S., M.S., and Ph.D degrees in Electrical Engineering from the Electrical Engineering Department of the University Basrah in 1999, 2005, and 2012, respectively. He is currently an assistant professor of Electrical Engineering at University of Basrah, Basrah, Iraq. His areas of interest include electrical machines drives and power electronics control. He can be contacted at email: ali.abdulabbas@uobasrah.edu.iq.



**Mazin Abdulelah Alawan**    was born in Basrah, Iraq in 1978. He received his bachelor degree in Electrical engineering from Basrah University, Iraq in 1999. He received MSc and PhD Degree in Electrical Engineering from Basrah University, Iraq in 2002 and 2012 respectively. He has joined Basrah University as lecturer in Computer Engineering department, and Shatt Alarab College University in Department of Computer Science. His primary research interest in digital protection system, modeling and simulation, electrical machines, intelligent control system, and renewable energy. He can be contacted at email: drmazinalwan@sa-uc.edu.iq.



**Diyah Kammel Shary**    was born in Basrah, Iraq in 1976. He received his bachelor degree in Electrical engineering from Basrah University, Iraq in 1999. He received MSc and Ph.D Degree in Electrical engineering from Basrah University, Iraq in 2002 and 2016 respectively. He has joined Southern Technical University as lecturer in Department of Electrical Power Techniques Engineering. His primary research interest in advanced power electronics, electrical machines, optimization techniques, intelligent controllers, and renewable energy systems. He can be contacted at email: diyahpower@stu.edu.iq.